The Journal of Chemical Physics

Oxygen activation on the interface between Pt nanoparticles and mesoporous defective TiO_2 during CO oxidation

Cite as: J. Chem. Phys. **151**, 234716 (2019); https://doi.org/10.1063/1.5131464
Submitted: 12 October 2019 . Accepted: 26 November 2019 . Published Online: 19 December 2019

Sunyoung Oh, Hyunwoo Ha, Hanseul Choi, Changbum Jo, Jangkeun Cho, Hyuk Choi, Ryong Ryoo, Hyun You Kim, and Jeong Young Park

AIP Publishing

The Journal of Chemical Physics ARTICLE scitation.org/journal/jcp

Oxygen activation on the interface between Pt nanoparticles and mesoporous defective TiO_2 during CO oxidation

Cite as: J. Chem. Phys. 151, 234716 (2019); doi: 10.1063/1.5131464
Submitted: 12 October 2019 • Accepted: 26 November 2019 •
Published Online: 19 December 2019

Sunyoung Oh,[1,2,a)] Hyunwoo Ha,[3,a)] Hanseul Choi,[1,2] Changbum Jo,[2] Jangkeun Cho,[2] Hyuk Choi,[3] Ryong Ryoo,[1,2,b)] Hyun You Kim,[3,b)] and Jeong Young Park[1,2,b)]

AFFILIATIONS

[1]Department of Chemistry, Korea Advanced Institute of Science and Technology (KAIST), Daejeon 34141, South Korea
[2]Center for Nanomaterials and Chemical Reactions, Institute for Basic Science (IBS), Daejeon 34141, South Korea
[3]Department of Materials Science and Engineering, Chungnam National University, Daejeon 34134, South Korea

Note: This article is part of the JCP Special Topic on Oxide Chemistry and Catalysis.
[a)]**Contributions:** S. Oh and H. Ha contributed equally to this work.
[b)]**Authors to whom correspondence should be addressed:** rryoo@kaist.ac.kr; kimhy@cnu.ar.kr; and jeongypark@kaist.ac.kr

ABSTRACT

Platinum-based heterogeneous catalysts are mostly used in various commercial chemical processes because of their high catalytic activity, influenced by the metal/oxide interaction. To design rational catalysts with high performance, it is crucial to understand the relationship between the metal–oxide interface and the reaction pathway. Here, we investigate the role of oxygen defect sites in the reaction mechanism for CO oxidation using Pt nanoparticles supported on mesoporous TiO_2 catalysts with oxygen defects. We show an intrinsic correlation between the catalytic reactivity and the local properties of titania with oxygen defects (i.e., Ti^{3+} sites). *In situ* infrared spectroscopy observations of the Pt/mesoporous TiO_{2-x} catalyst indicate that an oxygen molecule bond can be activated at the perimeter between the Pt and an oxygen vacancy in TiO_2 by neighboring CO molecules on the Pt surface before CO oxidation begins. The proposed reaction pathways for O_2 activation at the Pt/TiO_{2-x} interface based on density functional theory confirm our experimental findings. We suggest that this provides valuable insight into the intrinsic origin of the metal/support interaction influenced by the presence of oxygen vacancies, which clarifies the pivotal role played by the support.

I. INTRODUCTION

Catalytic oxidation of CO for Pt-based heterogeneous catalysis is a crucial reaction with growing practical importance in automotive catalysis and in the removal of CO from H_2 streams by preferential CO oxidation. This reaction is also important for understanding fundamental heterogeneous catalysis processes that include structure-sensitivity, active sites, and reaction pathways.[1–3] Enormous effort has been devoted to enhancing catalytic behavior by decreasing the size of nanoparticles (NPs) because of the significant role of metal–oxide interfaces in facilitating the catalytic conversion of adsorbed reaction species. Thus, metal–oxide interfaces have attracted attention as active sites because of the discovery of enhanced catalytic activity governed by geometric changes and charge transfer between the metal particles and the metal oxide support arising from the strong metal–support interactions (SMSI) suggested by Schwab.[4–7] The interfacial synergy of supported catalysts is generally based on the oxidation state, doping, and reducibility of the metal oxide support, which influences the catalytic performance.[8–11]

In oxidation reactions, both the adsorption and activation of molecular oxygen involved in CO oxidation have received attention as crucial steps in the catalytic performance of TiO_2-based catalysts.[12,13] In particular, the surface properties of TiO_2 (e.g., surface oxygen vacancies, steps, and interfaces) provide important characteristics that positively contribute to the catalytic activity of heterogeneous catalysts, photocatalysts, and gas sensors.[14–16] For

instance, the number of active oxygen species on Au/TiO_2 is related to the number of perimeter sites, signifying that the interfaces play a dominant role in O_2 activation.[17] Green and co-workers reported that O_2 bond dissociation is activated by the formation of a CO—O_2 complex at the perimeter of Au NPs surrounded by TiO_2 before CO oxidation occurs.[18,19] Furthermore, recent studies suggest that the role of surface vacancies is significant because of the formation of oxygen vacancies as dominant defect sites that can facilitate O_2 activation or electronic interaction with metal clusters.[20–22] Therefore, theoretical and experimental characterization clearly demonstrates the significance of the removal of oxygen (i.e., an oxygen vacancy) in TiO_2, which gives rise to Ti^{3+} centers that influence surface adsorption and the reactivity of key adsorbates (e.g., molecular oxygen or H_2O) on TiO_2.[23–26] O_2 molecules dissociate at vacant sites via one O atom healing the vacancy and another O atom bonding to the neighboring Ti site, as observed using STM.[27,28] In addition, H_2O dissociation on TiO_2 only takes place at bridging oxygen vacancy sites.[24,29] Despite extensive awareness of the crucial role of molecular oxygen adsorption and dissociation at the oxygen vacancy sites, understanding its involvement in CO oxidation is still in high demand and may improve or expand the scope of titania-based catalytic systems for specific applications.

Here, we synthesized a unique crystalline titania structure as a promising support using mesoporous TiO_2 with oxygen defect sites that was obtained using random-graft amorphous polymers without any complicated synthesis; Pt NPs were then deposited on this support via the $NaBH_4$ reduction method.[30] We investigated the correlation between the local properties of TiO_2 with oxygen defects and its catalytic performance in CO oxidation, which is based on the results of structural characterization and *in situ* infrared spectroscopy studies. The highest catalytic reactivity for the Pt/mesoporous TiO_{2-x} catalyst is related to the efficient activation of molecular O_2 at the interface between Pt and oxygen vacancy sites of the mesoporous TiO_{2-x}. Additionally, the ordered pore structure of the crystalline mesoporous TiO_{2-x} provides a novel method for enhancing highly dispersed metal NPs as well as sinter-resistant catalysts created by interfacial contacts, which all lead to improved catalytic activity. Subsequent density functional theory (DFT) calculations confirmed the close correlation between the CO oxidation performance of Pt/TiO_2 and the presence of oxygen vacancies. DFT-calculated CO oxidation pathways studied on Pt/TiO_2 with or without an oxygen vacancy provided theoretical insights into the chemical nature of the reaction site at the Pt/TiO_2 interface, which is sensitive to the local electronic structure change caused by an oxygen vacancy. These valuable results provide insight into the nature of the interaction between Pt NPs and the porous oxide support with oxygen vacancies and guidance toward rational designs for catalytic materials.

II. EXPERIMENTAL SECTION

A. Synthesis of Pt/mesoporous TiO_{2-x} and Pt/P25

Solvothermal synthesis of the mesoporous TiO_{2-x} was performed using poly(4-vinylphenol-*co*-methyl methacrylate) (PVP-*co*-PMMA, Sigma-Aldrich) in a dimethylformamide (DMF) solution. In brief, 0.72 g of PVP-*co*-PMMA was dissolved in 25 ml of DMF with magnetic stirring. 0.67 ml of titanium(III) chloride ($TiCl_3$, Aldrich, 99.9%, TiO_2 precursor) was added dropwise to the prepared solution with vigorous stirring. The solution was heated at 100 °C for 1 h to completely form phenol—Ti—O bonds.[31] 0.33 ml of deionized water was then added dropwise to this solution, and 3.4 ml of distilled triethylamine was subsequently added to neutralize the solution. The mixture was transferred into a Teflon-lined autoclave and then heated in an oven at 150 °C for 3 days. The product was collected using centrifugation and dried in a convection oven at 100 °C. After calcination in air at 350 °C, the mesopores were opened by decomposition of the polymer. A trace amount of the remaining carbonaceous residue in the sample was completely removed with ozone flow at 260 °C for 4 h.[30]

The $NaBH_4$ reduction process was used to prepare the Pt NPs deposited on the mesoporous TiO_2 support with oxygen defects.[32] First, 0.2 g of mesoporous TiO_2 with oxygen defects was dissolved in 500 ml of deionized (DI) water with subsequent vigorous stirring at room temperature for 30 min. Then, 250 ml of a chloroplatinic acid hexahydrate ($H_2Cl_6Pt{\cdot}6H_2O$, Aldrich) solution dissolved in deionized H_2O was stirred and added drop by drop into the prepared mesoporous TiO_{2-x} solution, followed by stirring. After that, a freshly prepared $NaBH_4$ solution (0.5M dissolved in deionized H_2O) was added dropwise into the mixed solutions of the Pt precursor and TiO_{2-x} support to reduce the metal precursor and attach the Pt NPs onto the TiO_{2-x} support. After an additional 24 h of stirring, the resulting catalyst was filtered and washed with DI water until no Cl^- remained and then dried for 24 h at 80 °C in an oven. To compare the effectiveness of the mesoporous TiO_{2-x} and Degussa P25 (commercial support), we prepared Pt NPs supported on Degussa P25 powder with the method adopted from the $NaBH_4$ reduction method mentioned above. Following several repetitions of the washing process, weakly adsorbed Pt and other ions were washed off to ensure strong deposition of the Pt NPs on the mesoporous TiO_{2-x} and P25 supports.

B. Characterization of Pt NPs deposited on TiO_2 supports

The Pt compositions in the supported Pt catalysts (i.e., Pt/mesoporous TiO_{2-x} and Pt/P25) were measured using inductively coupled plasma mass spectroscopy (ICP-MS; Perkin Elmer, DRC-e model). The surface areas and pore size distributions of the prepared catalysts were obtained using the Brunauer–Emmett–Teller (BET) method with the adsorption of N_2 at the temperature of liquid nitrogen. The morphologies and size distributions of the supported Pt catalysts were performed using TEM operated at an acceleration voltage of 300 kV (Tecnai TF30 ST, FEI). Scanning transmission electron microscopy (STEM) images of the Pt/mesoporous TiO_{2-x} catalysts were obtained using a Titan Double Cs corrected TEM at an acceleration voltage of 300 kV. Prior to the measurements, the catalysts were well-dispersed in an ethanol solution for 60 min, followed by drop-casting on an amorphous carbon-coated TEM grid, and then dried for a few minutes. X-ray powder diffraction (XRD, Rigaku D/MAX-2500 at 40 kV, 300 mA) was used to analyze the crystal structure. Raman spectra were collected on a LabRam HR Evolution microscope. The chemical bonding states of the supported Pt catalysts were further examined using XPS (K-alpha, Thermo VG Scientific) equipped with an Al Kα X-ray source (1486.3 eV).

C. Catalytic oxidation performance of carbon monoxide

The CO oxidation reaction was conducted with the prepared Pt supported catalysts in a flow reactor equipped with a gas chromatograph (GC; DS science) with a thermal conductivity detector (TCD) for analyzing the gas mixture. Prior to the reaction, 50 mg of the catalyst was loaded in a quartz tube followed by reduction at 250 °C under H_2 flow (5% H_2 balanced with He, 45 ml/min) for 30 min and then cooled to room temperature. The reactant mixture consisted of 4% CO and 10% O_2 balanced with He. The total gas flow rate was kept at 50 ml/min using mass flow controllers (MFC, BROOKS Instrument). The gas hourly space velocity of the reaction (GHSV) was 30 000/h. The reaction was performed from 30 to 210 °C, and the temperature was increased 5 °C/10 min, while consecutively monitoring the reactant and product concentrations. The CO oxidation reaction continued until the CO was completely converted to CO_2.

D. DRIFTS experiments

The *in situ* infrared (IR) measurements were performed on an Agilent Carry 660 spectrometer equipped with integrated diffuse reflectance optics (Harrick), a *l*-N_2 cooled mercury cadmium telluride (MCT) detector, and a ZnSe window integrated reactor cell made of stainless steel. All the spectra were recorded using 32 scans and a resolution of 4 cm^{-1}. The IR reactor cell was connected to a heater to vary the temperature. Different mixtures of gases were introduced into the IR reactor cell, and the flow rates were controlled by MFC. All prepared samples were mechanically pressed into a cleanly prepared stainless-steel mesh to prevent potential contamination exposure in the reactor cell. Before the measurements, the catalyst was pretreated with 100 SCCM of 5% H_2/He at 250 °C for 1 h and then cooled to room temperature (27 °C) in He.

All the prepared catalysts were monitored using diffuse reflectance infrared fourier transform spectroscopy (DRIFTS) and a quadruple mass spectrometer (QMS). For the CO oxidation reaction, the gas mixture (1% CO/4% O_2/He, 50 ml/min) was simultaneously introduced into the reactor cell for 30 min to ensure steady-state reactivity. A reference spectrum taken through the catalysts in the He gas environment was subtracted from every spectrum recorded for the samples under the CO oxidation conditions. The spectral results were converted using the Kubelka–Munk function.

E. Density functional theory calculations

A diagonal 3 × 4 slab (surface vectors of [1 −1 −1] and [0 1 0]) with three layers of TiO_2 was used to describe the anatase TiO_2(101) surface.[33] An fcc-type Pt_9 NP was deposited on TiO_2(101) and initially optimized. The bottom TiO_2 layer was fixed during all calculations. The preoptimized Pt_9/TiO_2 models were applied to the subsequent DFT-molecular dynamics (DFT-MD) simulation to obtain an initial Pt/TiO_2 structure for the DFT-based catalytic performance analysis. A DFT-MD simulation was performed at 1000 K for 1.5 ps of the total production time with a 1 fs of the time step. This model with a Pt_9 NP on stoichiometric TiO_2(101) [i.e., Pt_9/TiO_2(101)] stands in for the experimentally synthesized Pt/P25. To describe the atomic structure of the reaction sites of Pt/TiO_{2-x}, an oxygen vacancy was formed at the interface between the Pt_9 and TiO_2(101) [i.e., Pt_9/TiO_{2-x}(101)] (see Fig. S1 of the supplementary material).

We performed spin-polarized DFT calculations using a plane-wave basis with the Vienna *ab initio* simulation package (VASP) code.[34,35] The exchange-correlation potential was functionalized by the PW91 scheme.[36] To appropriately treat the localized Ti *d*-orbitals, DFT+U[37] with U_{eff} = 4.5 eV was applied to the Ti ions.[38] The interaction between the ionic core and the valence electrons was described by the projector augmented wave method, and the valence

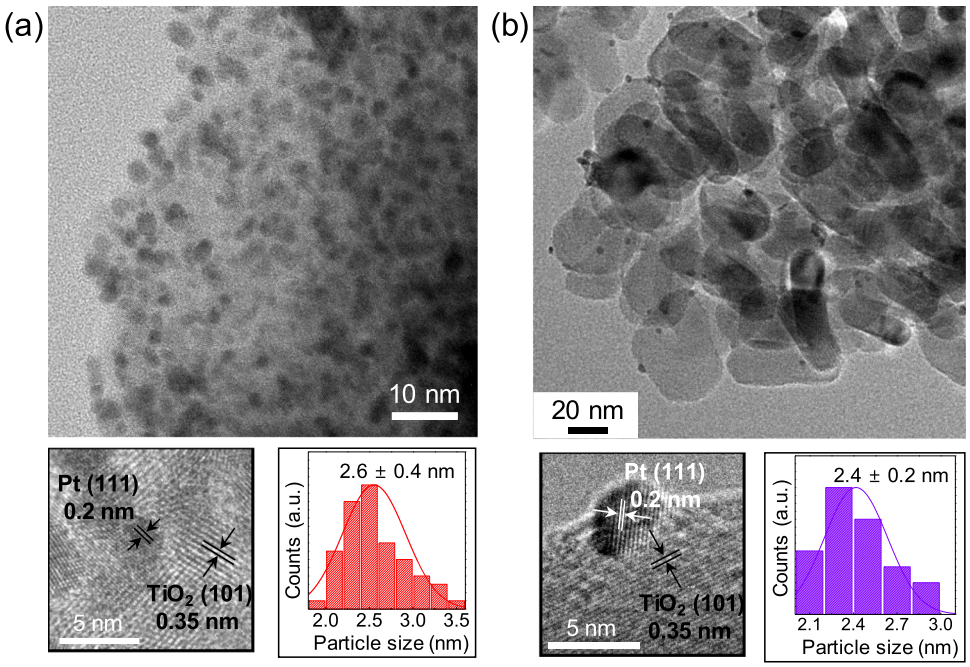

FIG. 1. HRTEM images, Pt nanoparticle size distribution histograms, and the exposed facets of the Pt and TiO_2 in corresponding TEM images for the (a) Pt/mesoporous TiO_{2-x} and (b) Pt/P25 catalysts.

electrons were treated on a plane wave basis up to an energy cutoff of 400 eV. The Brillouin zone was sampled at the Γ-point. The convergence criteria for the electronic structure and geometry were 10^{-3} eV and 0.03 eV/Å, respectively. We used the Gaussian smearing method with a finite temperature width of 0.2 eV to improve the convergence of states near the Fermi level. The location and energy of the transition states (TSs) were calculated using the climbing-image nudged elastic band method.[39,40]

III. RESULTS AND DISCUSSION

A. Structural characterization of supported Pt catalysts

All the supported Pt catalysts were investigated using TEM (Fig. 1), which displays the Pt NPs loaded on crystalline mesoporous TiO_{2-x} and P25 supports; the Pt NPs were uniformly deposited on the different structures of the oxide supports. The mean diameter of the Pt NPs for the prepared catalysts is quite narrow at 2 nm from the size distribution histograms. High-resolution (HR) TEM images can easily resolve the crystal lattice of both the TiO_{2-x} and Pt NPs; this allows for confirmation of the sample morphology [Fig. 1(a)]. To clearly recognize the nanostructures, we obtained high-angle annular dark-field scanning transmission electron microscopy (HAADF-STEM) images and corresponding energy dispersive X-ray spectroscopy (EDS) phase mappings (Fig. S2). The pore size distribution derived from the adsorption isotherm indicated a sharp distribution centered at a diameter of 3.5 nm (Fig. S3). Furthermore, the Pt compositions were 0.7 and 1.0 wt. % for Pt/TiO_{2-x} and Pt/P25, respectively (Table S1). The surface area of the prepared Pt catalysts using the TiO_{2-x} support examined by the BET method is quite high compared with other normal oxides, including P25 (Table S1).[41] The structural information for the as-synthesized Pt catalysts is shown in the X-ray diffraction patterns in Fig. 2(a), implying that all the diffraction peaks can be indexed to the anatase phase of TiO_2, the crystalline TiO_{2-x}, and the mixed rutile and anatase phases of P25.[42] After depositing the Pt on the oxide supports, there are no diffraction peaks for Pt-containing crystal phases because the Pt NPs are highly dispersed on the surface of the TiO_2 with a small particle size (typically <5 nm), which cannot be detected by Bragg diffraction.[43] As shown in Fig. 2(b), Raman spectra were measured to explore the crystal structure and surface compositions of the Pt/TiO_{2-x} and Pt/P25 catalysts. The five Raman-active modes of the anatase phase, with frequencies at 144 (E_g), 197 (E_g), 396 (B_{1g}), 514 (A_{1g}), and 636 cm^{-1} (E_g), were consistent with the characteristic peaks of the anatase TiO_2 phase; they were confirmed using XRD analysis.[44] Compared with the Pt/P25 catalyst, the two Eg modes for the Pt/TiO_{2-x} are blue shifted by 5 and 4 cm^{-1}, respectively, which is attributed to atomic rearrangement because of the defective TiO_{2-x} layer.[45] Moreover, the XPS spectra for the Ti 2p

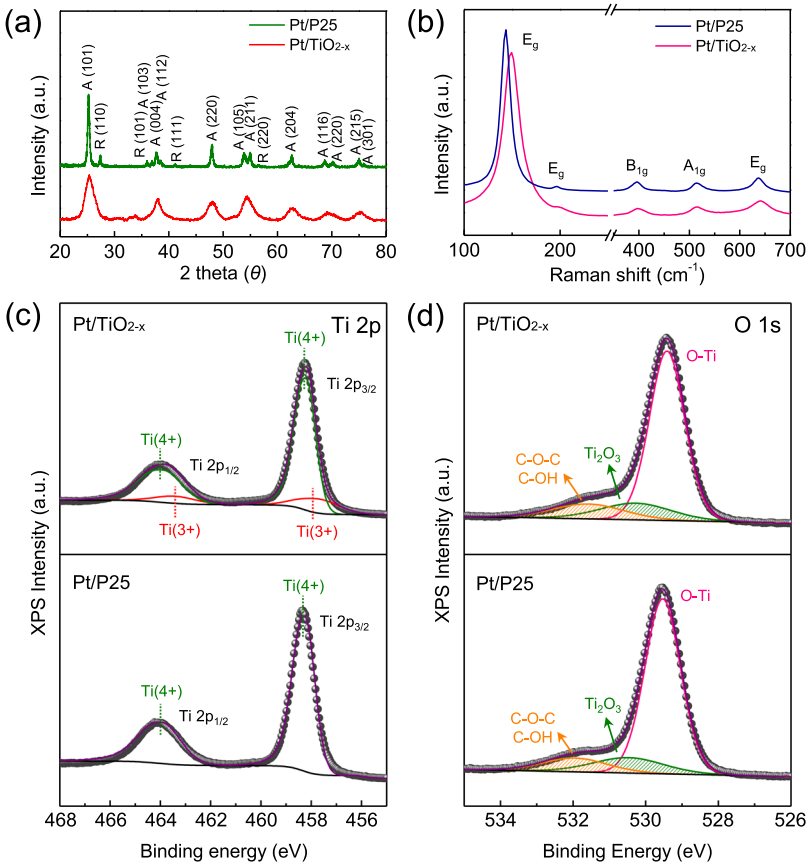

FIG. 2. (a) XRD patterns, (b) Raman spectra, (c) XPS spectra of Ti 2p, and (d) of O 1s for the Pt/TiO_{2-x} and Pt/P25 catalysts.

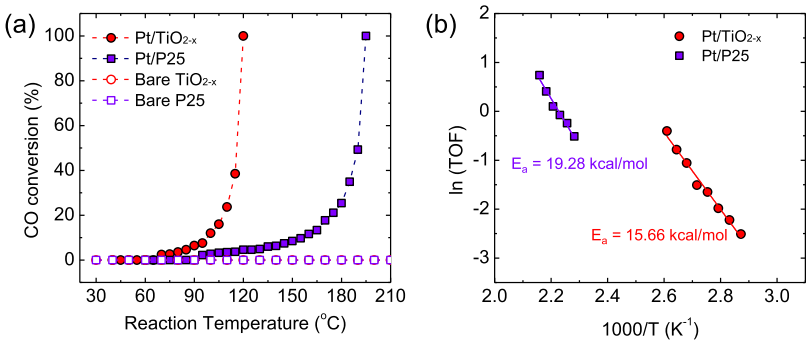

FIG. 3. Comparison of the temperature-dependent CO conversion on (a) Pt NPs supported on different oxides (TiO_{2-x} and P25) and the corresponding bare oxides. (b) Arrhenius plot of the TOF of the corresponding Pt/TiO_2 catalysts.

and O 1s regions of these samples are indicated in Figs. 2(c) and 2(d). The XPS spectra were deconvoluted into the individual components. For the Pt/P25 catalyst, the Ti^{4+} $2p_{1/2}$ and Ti^{4+} $2p_{3/2}$ are located at 463.9 and 458.2 eV, respectively [Fig. 2(c)]. However, there are two additional fitting peaks for Ti^{3+} at 463.4 and 457.7 eV for the Pt/TiO_{2-x} catalyst, signifying that the existence of the Ti^{3+} state is related to the stoichiometry deficiency of the oxide.[46] The binding energies of Ti^{4+} $2p_{3/2}$ and Ti^{3+} $2p_{3/2}$ for the supported Pt catalysts are listed in Table S2. The O 1s spectra were acquired for the Pt/TiO_{2-x} and Pt/P25 samples [Fig. 2(d)], and the main peak is for the O—Ti bonds. The atomic ratios were determined on the basis of the O 1s spectrum (Table S2). In Pt/TiO_{2-x}, the O_{Ti2O3} atomic ratio is higher and the O_{O-Ti} atomic ratio is lower than the corresponding values in Pt/P25. All the results of the structural characterization of the Pt/TiO_{2-x} catalyst suggest the formation of oxygen-deficient anatase TiO_2 compared with P25. One plausible mechanism for the formation of oxygen vacancies is that negatively charged −C=O bonds in PVP-*co*-PMMA prefer to bind to positively charged and unsaturated Ti^{4+} ions during the nucleation process to reduce surface energy. The PVP-co-PMMA hinders Ti^{4+} from binding to oxygen, which could lead to the generation of abundant oxygen vacancies during the calcination process.[47,48] Therefore, the oxygen vacancies may be expected to play an important role in the oxidation reactions.

B. Catalytic reaction performance

The CO oxidation reaction was performed in a flow reactor at atmospheric pressure on pure titania-based supports (i.e., mesoporous TiO_{2-x} and P25), as well as with the Pt NPs deposited on their oxides at temperatures between 30 and 210 °C, following reductive pretreatment to identify the intrinsic origin of the metal–support interfaces dependent on the different local morphologies and surface compositions of the TiO_2 supports (Fig. 3). The CO conversion was attained for different TiO_2 supports [Fig. 3(a)], which shows that the observed catalytic activities for the supported Pt catalysts are considerably higher than for the bare TiO_2 supports (i.e., mesoporous TiO_{2-x} and P25). It was reported that the metal–oxide interface provides reactive catalytic sites with enhanced activity by depositing Pt NPs on TiO_2 supports.[49] Residual surface Cl on the supported Pt catalysts was excluded as the main cause of the difference in activities (Fig. S4). The higher activity for CO oxidation on the Pt/mesoporous TiO_{2-x} than on Pt/P25 suggests that the novel mesoporous structure is an effective support because of its many unique physicochemical properties (e.g., high surface area, high metal dispersion, outstanding thermal stability, and uniform pore size) compared with nonporous oxides.[8,50–52] Highly crystalline mesoporous oxides provide a high proportion of active interface sites and facilitate the adsorption and diffusion of reactant molecules compared with bulk oxides.[53] Moreover, the presence of oxygen vacancies for the unique TiO_{2-x} structure (Fig. 2) may influence and boost the catalytic performance for CO oxidation.

The corresponding Arrhenius plots of the TOFs on the TiO_2-based catalysts with deposited Pt NPs are shown in Fig. 3(b). The apparent activation energies extracted from the slopes of the curve were calculated to be 15.66 and 19.28 kcal/mol for Pt/TiO_{2-x} and Pt/P25, respectively (Table I). It is therefore of interest to understand how differences in the local structure of the TiO_2 support, as well as the active interface sites between the Pt and oxygen vacancies in the TiO_2, may influence the catalytic activity for CO oxidation. Therefore, the rational design of supported noble-metal catalysts could maximize the dispersion of the active sites of the noble metals, thus improving the catalytic activity by using porous oxide supports. A

TABLE I. Results of ICP, BET, and CO oxidation for Pt/TiO_{2-x} and Pt/P25 catalysts.

Sample	Metal composition (wt. %)	BET surface area (m^2/g)	Metal surface area per metal weight (m^2/g_{Pt})	T_{100} (°C)	Activation energy (kcal/mol)
Pt/TiO_{2-x}	0.7	230.0	0.496	120	15.66
Pt/P25	1.0	56.8	0.206	195	19.28

plot of the Pt 4f peaks of Pt/TiO_{2-x} and Pt/P25 before and after the CO oxidation reaction reveals that the value of Pt 4f after CO oxidation is slightly shifted to a higher binding energy (Fig. S5). The chemical shift of the Pt 4f peak reveals higher oxidation states, which refer to the formation of Pt oxide and show that molecular oxygen can be activated on supported Pt catalysts.

It is generally understood that the structure phase affects catalytic reactivity. As shown in Fig. 2(a), P25 is composed of a mixture of anatase and rutile structures, whereas mesoporous titania is mainly composed of the anatase phase. However, we can rule out that the difference in the crystal structure could influence the catalytic reactivity from results in the literature.[54] Di *et al.* prepared Au/P25 and Au/TiO_2, which consist of anatase only, and they compared the catalytic reactivity by CO oxidation reaction. Although 100% conversion was achieved above 60 °C with both catalysts, the Au/TiO_2 (anatase) catalyst showed lower catalytic reactivity at lower temperatures. Therefore, we can exclude the crystal structure effect on catalytic reactivity.

C. *In situ* DRIFTS studies

To further understand the observed behaviors underlying the enhancement of the catalytic activity for Pt/TiO_{2-x}, *in situ* characterization using DRIFTS was conducted under catalytically relevant reaction conditions. Identification of the intermediates using vibrational spectroscopy methods with CO was indispensable because IR techniques provide a sample-averaged quantitative measure of many relevant properties (e.g., local structure, oxidation state, and coordination environment).[43,44]

Contour maps of the supported Pt catalysts visualize an intriguing observation of the IR bands that corresponds to CO adsorption on the Pt NPs and evolution of CO_2 molecules under CO oxidation conditions (Fig. 4). The linear CO adsorbed on Pt^{2+} (oxidized cationic Pt; 2107 cm^{-1}) and on $Pt^{\delta+}$ and Pt^0 sites (2081–2054 cm^{-1}) was distinctly observed, which is similar to the previous reports.[55,56] The Kubelka-Munk (KM) absorbance units are related to the proportional adsorbate surface concentration when accounting for strongly absorbing surface species.[57] The CO stretching bands of the Pt/P25 catalyst give sharper infrared bands at higher frequencies than Pt/TiO_{2-x}, which is consistent with the tendency of NPs to sinter during reaction compared with Pt NPs supported on mesoporous TiO_{2-x} (Fig. S6). This propensity reflects the combined effects of M–C strength and the alignment of the CO dipoles on the well-coordinated atoms prevalent in larger clusters, as reported in previous studies.[58,59] The IR peak of the adsorbed CO on the Pt surface ($Pt^{\delta+}$ and Pt^0) is also shifted to a higher frequency depending on the oxidation state of the Pt NPs, which is caused by the reduced back-donation effect that originates from the difference in a small quantity of d-electrons for the adsorbate-induced Pt sites compared with the metallic Pt surface.[60] This is in agreement with the presence of a more oxidized Pt surface for Pt/P25 catalysts, as seen in the XPS results (Fig. S5). However, CO adsorbed on a TiO_2 surface was not observed (at ~27 °C), which corresponds well with previous reports of weak CO chemisorption on the TiO_2 surface above 25 K.[61]

IR spectroscopy observations at specific temperatures of the Pt/mesoporous TiO_{2-x} and Pt/P25 catalysts are shown in Fig. 5. The experimental spectra for all the CO bonding to the Pt sites were fitted with Gaussian peaks to observe any variation of their relative amounts, which are attributed to linearly adsorbed CO on Pt^{2+} (oxygen on Pt), $Pt^{\delta+}$ (oxygen on neighboring Pt), and Pt^0 sites.[62–65] In general, the CO-induced restructuring of Pt NPs supported on irreducible oxides (e.g., SiO_2 and Al_2O_3) under CO oxidation reaction conditions comes from an increase in the stretching frequency, as the CO is bound to undercoordinated Pt sites at 2080–2098 cm^{-1}.[66] However, in the Pt/TiO_{2-x} catalyst, the spectral peak at 2107 cm^{-1} (referring to oxidative Pt) emerges abruptly at 126 °C, as shown in Fig. 5(a). The observed higher wavenumber is not associated with the increased NP size governed by a decrease in the amount of π-back-donation into the C≡O, as reported in the literature.[67] The Pt/mesoporous TiO_{2-x} catalyst with thermal stability exhibited a higher reaction rate than that of the Pt/P25 catalyst, while preserving high immobilization stability of the Pt NPs during the reaction process (Fig. S6). This demonstrates that the Pt atom may be placed on an oxygen vacancy generated on the reduced TiO_2 surface caused by the reductive pretreatment.[68] The strong metal–support interaction suppresses the metal sintering reported by Farmer and Campbell.[69]

The significant spectral evidence for the emergence of a new intense peak at 2107 cm^{-1} was attributed to the higher amount of O in the vicinity of Pt, leading to a lower electron density caused by reduced back-donation from the Pt site to the antibonding

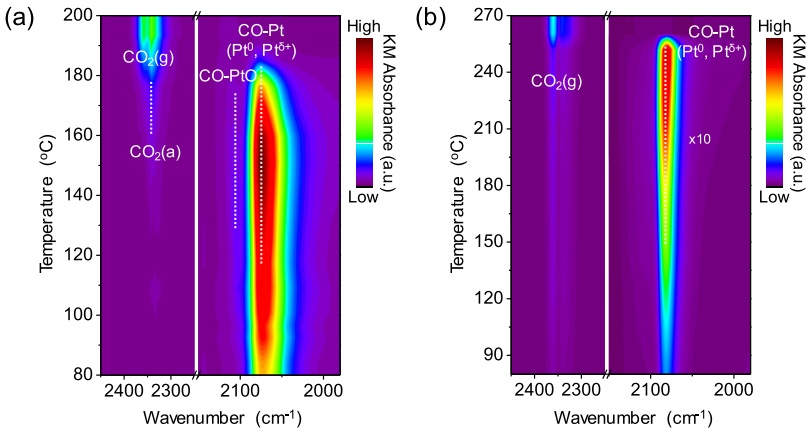

FIG. 4. *In situ* DRIFT spectra measured on the supported Pt catalysts. A narrower spectral range is presented as a 2D contour map for the (a) Pt/TiO_{2-x} catalyst and (b) Pt/P25 catalyst under a flow of 1% CO/4% O_2/He at elevated temperatures. All the catalysts were reduced at 250 °C in H_2 prior to CO oxidation. Spectra plotted in arbitrary units of KM absorbance.

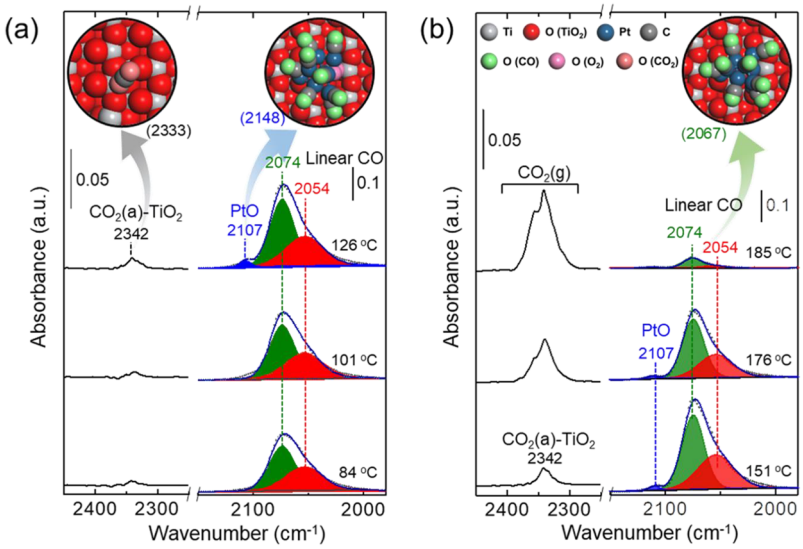

FIG. 5. IR spectroscopy observations of the site-specific signatures of CO adsorbed onto different Pt sites (i.e., PtO, $Pt^{\delta+}$, and Pt^0) and the produced CO_2 with DFT-calculated stretch frequencies of the adsorbed CO and CO_2 molecules for the (a) initiation and (b) activation of CO oxidation on the Pt/mesoporous TiO_{2-x} catalyst as a function of temperature. The numbers in the parentheses present the DFT-calculated IR frequencies.

molecular orbital of CO [Fig. 5(a)]. First, there is the possibility that molecular oxygen can simultaneously adsorb to both the oxygen vacancy sites of the TiO_{2-x} (Fig. 2) and the Pt surface adjacent to the perimeter. Yates *et al.* reported that molecular oxygen can adsorb on a defective TiO_2 surface because O_2 does not adsorb on a TiO_2 surface unless surface oxygen vacancies are present.[70,71] The previously adsorbed CO molecule on the Pt surface then induces the dissociation or activation of the molecular oxygen adsorbed on the interface between the Pt surface and the defective TiO_2. Thus, the peak at 2342 cm^{-1}, which is the characteristic for physisorbed CO_2 on TiO_2, forms as a result of the CO oxidation reaction and the associated CO spillover from the Pt surface to O_2 adsorbed at the interface.[72–74] Interestingly, the coexistence of PtO species (2107 cm^{-1}) can demonstrate chemisorbed oxygen on the Pt surface that originates from a dissociated O atom at the interface between the Pt and the oxygen vacancy sites of the mesoporous TiO_{2-x}. It is well known that CO oxidation occurs via CO assisting in the dissociation of O_2 to form reactive $O^*-O-C^*=O$ intermediates that decompose both chemisorbed oxygen and CO_2.[58] We note that the coexistence of PtO species is correlated with the oxidized Pt surface of the Pt nanoparticles caused by CO-assisted oxygen dissociation, which is not related to a single Pt atom, because the Pt nanoparticles were confirmed by HAADF-STEM (Fig. S2).[75] In addition, after the CO oxidation reaction, the oxidation states of Pt 4f for the Pt/TiO_{2-x} show the existence of Pt^{4+} species, indicating that molecular oxygen can be activated or dissociated at the interfacial sites (Fig. S5).

These spectral observations of the PtO species also indicate that the CO oxidation reaction occurs as a function of temperature because the Pt cations, as supported metal cations, cause weakened Pt—CO bonds and CO desorption, thus improving the catalytic activity originating from Pt sites without strongly adsorbed CO.[76] At higher temperatures (i.e., above 151 °C), the IR peaks of the linear CO adsorbed on the Pt surface (i.e., $Pt^{\delta+}$ and Pt^0)—including CO adsorbed on Pt^{2+} species—steadily decreased [Fig. 5(b)]. The decrease in the linear CO stretching peaks can be explained by the chemisorbed oxygen (from CO-assisted O_2 dissociation) on Pt adjacent to the interface reacting with a neighboring CO molecule on the Pt surface, which is the activation step for CO oxidation.[77] Thus, the formation of an activated platinum–oxygen complex on the mesoporous TiO_{2-x} support at high temperature contributes to the high catalytic activity. To explain the CO oxidation rates, the gas-phase CO_2 product (as observed by the doublet peak at 2300–2380 cm^{-1}) on the Pt/TiO_{2-x} for CO oxidation was calculated by integrating the absorbance of the CO_2 in the IR spectra and monitored by QMS as a function of temperature (Fig. S7). It appears that the CO oxidation activity and the IR area of the CO_2 peak increase simultaneously. An Arrhenius analysis of the rate of CO_2 formation on the Pt/TiO_{2-x} from the QMS data yields an apparent activation energy of 15.58 kcal/mol, which agrees with the results from the CO oxidation reaction in the flow reactor system. A definitive correlation between the sample-averaged quantitative measurement of CO-assisted O_2 dissociation by infrared spectroscopy and the reaction rate strongly demonstrates that the activation of molecular oxygen is dependent on the interface between the Pt surface and an oxygen vacancy site in the TiO_{2-x} support. Molecular oxygen adsorption and dissociation over supported catalysts using a TiO_2 support are generally considered a key step in CO oxidation because only a TiO_2 support cannot activate O_2.[19] Recently, theoretical results of CO oxidation on Au/TiO_2 have showed that O_2 can be easily activated at the interface boundary, leading to an oxidized interface.[78] The number of reactive oxygen species generally present on the metal/support interface is linearly related to the number of perimeter sites at the metal–support interface, showing that the interface plays a dominant role in O_2 activation.[79] There are also extensive studies showing that the oxygen lattice on reducible oxides (e.g., TiO_2 and CeO_2) can participate in the reaction via the Mars–van Krevelen (M–vK) mechanism.[80–83] Nonetheless, the mechanisms for CO oxidation on supported catalysts and for oxygen adsorption and activation remain controversial.

For comparison, we performed DRIFTS investigations of the prepared Pt/P25 catalyst under the same conditions (Fig. S8). For Pt/P25, the IR absorption of linear CO adsorbed on the Pt surface was also detected as a function of temperature, along with the production of CO_2 gas molecules. However, the intriguing features [i.e., CO-Pt^{2+} and CO_2(a)-TiO_2] of the Pt/TiO_{2-x} catalyst are absent, and the reaction temperature is higher than that for the Pt/TiO_{2-x} catalyst. Additionally, the activation energy for the Pt/P25 catalyst is 20.45 kcal/mol (calculated from the QMS results while simultaneously measuring IR), which is higher than the activation energy for the Pt/TiO_{2-x} catalyst. These results clearly reveal the importance of the existence of Ti^{3+} sites (or oxygen vacancies) for the CO oxidation reaction; thus, the enhancement of the adsorption and activation of oxygen molecules causes higher catalytic reactivity. Moreover, the ordered mesoporous structures of the transition metal supports (i.e., the unique mesoporous TiO_{2-x} structure) offer greater internal and external surfaces for effective Pt NP dispersion, generating a larger oxide–metal interface.[8] Therefore, molecular oxygen can be effectively activated by diffusion of the CO species at the larger oxide–metal interface sites, which promotes catalytic activity. The O_2 activation phenomena that take place at the interface between the Pt and defective TiO_2 sites by CO spillover were probed with *in situ* IR spectroscopy, which allows us to believe that the use of mesoporous TiO_2 with oxygen vacancies enhanced the catalytic properties.

D. DFT-calculated CO oxidation pathways by Pt/TiO_2(101) and Pt/TiO_{2-x}(101)

To provide a theoretical interpretation of the key experimental observations of the improved CO oxidation properties of the Pt/mesoporous TiO_{2-x}, we constructed the CO oxidation pathways catalyzed by Pt_9/TiO_2(101) and Pt_9/TiO_{2-x}(101), which represent Pt/P25 and Pt/TiO_{2-x}, respectively. Based on our experimental findings, an oxygen vacancy was located at the Pt-TiO_2 interface of the Pt_9/TiO_2(101) to generate the Pt_9/TiO_{2-x}(101) model. This oxygen vacancy significantly strengthened Pt-TiO_2 adhesion by increasing the electronic interaction between the Pt NPs and the excess electrons localized at the oxygen vacancy in the TiO_2 (Fig. S1). This strengthening effect may lead to the experimentally observed enhanced thermal stability of the Pt NPs supported on the defective TiO_2 structure (Figs. 1 and S6). In our recent consecutive DFT studies of CO oxidation by Au NPs supported on CeO_2[80,84] and Pt-Cu bimetallic NPs,[85] we applied the CO-covered NP models to more precisely describe the catalyst surface under CO oxidation conditions. To find the energetically available CO and O_2 coverage of our Pt/TiO_2 models, we calculated the sequential CO binding energy of the Pt NP of Pt_9/TiO_2(101) and found that the Pt_9 NP of Pt_9/TiO_2(101) prefers to bind up to 8 CO molecules and a final O_2 molecule (Fig. S9a). The energetic trend of sequential competitive CO and O_2 binding on Pt_9/TiO_2(101) shows that the E_{bind} values for the first 8 CO molecules (≥−1.19 eV) are stronger than the E_{bind} of a single O_2 molecule (−0.89 eV) on bare Pt_9, meaning that a large portion of the surface of the Pt NPs supported on TiO_2 will be covered by CO (Fig. S9a). However, an interesting inversion was observed in the energetics of the last binding molecules, as the E_{bind} of O_2 (−2.15 eV) exceeds the E_{bind} of the 9th binding CO molecule (−1.22 eV) (Figs. S9a and S9b). This inversion, the occupation of the last binding site by O_2 rather than CO, was concurrently found in the Pt_9/TiO_2(101) (Figs. S9b and S9c) and Pt_9/TiO_{2-x}(101) (Figs. S9d and S9e) models. The last binding O_2 molecule on Pt_9/TiO_2(101) was bound to the Pt-TiO_2 interface, bridging the Ti ion and the interfacial Pt atom. On the other hand, the last-bound O_2 molecule on Pt_9/TiO_{2-x}(101) healed the oxygen vacancy at the Pt-TiO_2 interface. The excessively elongated O—O bond of the O_2 in Pt_9/TiO_{2-x}(101) (1.484 Å) shows that this O_2 molecule is electronically enriched and can therefore be relatively easily utilized for CO oxidation (Fig. S9e).

From our experimental observations of the catalytic activity of Pt NPs supported on mesoporous TiO_{2-x}, we identified the

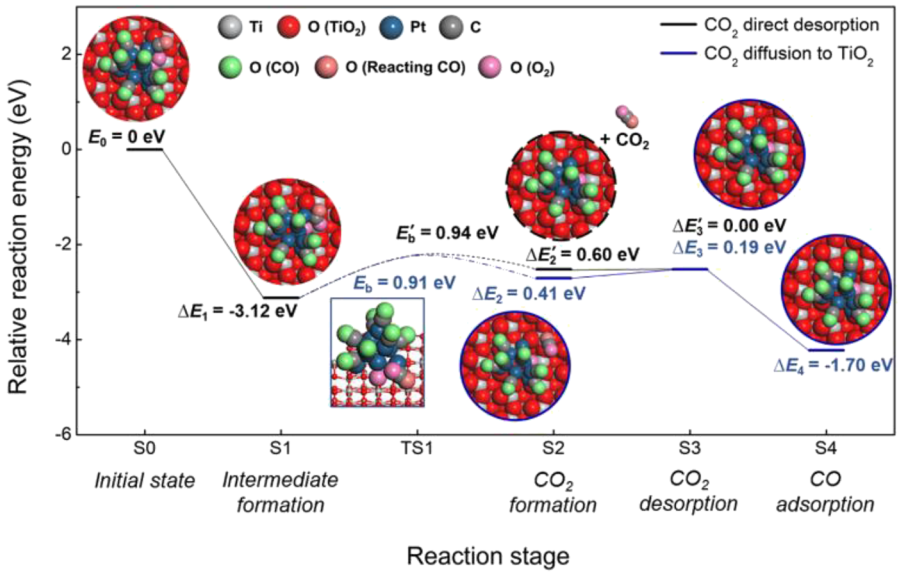

FIG. 6. DFT-constructed CO oxidation pathways catalyzed by Pt/TiO_{2-x} with eight adsorbed CO and one adsorbed oxygen molecule (state 0, S0) show that CO_2 desorption occurs at the Pt_9-TiO_{2-x}(101) interface (black line) or on the TiO_2(101) surface (blue line). ΔE_n represents the reaction energy calculated by comparing the absolute energies of stage n and stage $n-1$. E_b denotes the activation energy barrier. The comparable ΔE_2 and $\Delta E'_2$ values predict that direct CO_2 desorption (black line) or CO_2 diffusion to an adjacent Ti ion (blue line) are possible.

interface between Pt and TiO_{2-x} as a reactive site for catalytic CO oxidation. The overall CO oxidation pathway catalyzed by $Pt_9/TiO_{2-x}(101)$ presented (Fig. 6) shows that the interface-bound O_2 molecule indeed oxidizes an adjacent Pt-bound CO molecule. The O_2 molecule at the Pt-$TiO_{2-x}(101)$ interface was easily dissociated by an adjacent CO molecule, presenting the reaction through CO-assisted O_2 dissociation. Two kinds of CO_2 production pathways (from S1 to S3, Fig. 6)—direct desorption of CO_2 from Pt NPs (black-colored pathway, $\Delta E_n'$) and CO_2 diffusion from the Pt NPs to the TiO_2 and subsequent desorption (dark blue-colored pathway, ΔE_n)—were energetically available with almost identical energy barriers of 0.94 eV (direct CO_2 desorption from Pt) and 0.91 eV (two-step diffusion–desorption process). The DFT-calculated CO_2 stretch frequency of the CO_2 adsorbed on the $TiO_{2-x}(101)$ (stage S2, Fig. 6) was 2333 cm^{-1}, which is equivalent to the experimental frequency of CO_2(a)-TiO_2 at 2342 cm^{-1} [Fig. 5(a)]. The blue shifted experimental CO stretch frequency observed at 2104 cm^{-1} assigned to PtO-bound CO molecules was also reproduced with the Pt-bound CO molecules (2148 cm^{-1}), which are adjacent to the Pt-TiO_{2-x} interface-bound O_2 molecule. The experimental IR peak centered at 2074 cm^{-1}, for Pt-bound linear CO molecules, was reproduced by the DFT calculations [2067 cm^{-1}, Fig. 5(b)]. The DFT-constructed reaction pathways and the IR frequencies confirm our experimental findings of vacancy-assisted CO oxidation at the Pt-TiO_{2-x} interface. On the other hand, we found that the three different O_2 activation pathways examined on $Pt_9/TiO_2(101)$ are highly thermodynamically uphill (M-vK type of CO oxidation, black-colored pathways, Fig. S10) or kinetically slow. The high activation energy barriers of CO-assisted O_2 dissociation (1.32 eV) and direct O_2 dissociation (1.47 eV) presented (Fig. S10) predict that the activation of the O_2 molecule adsorbed at the Pt-$TiO_2(101)$ interface slows without an oxygen vacancy. Although our DFT-calculated CO oxidation pathway shows that the initially formed oxygen vacancy at the Pt_9-TiO_{2-x} interface was healed upon O_2 adsorption and CO oxidation (Fig. 6), we believe that oxygen vacancies will be dynamically and spontaneously formed at the Pt-mesoporous TiO_{2-x} interfaces under real CO oxidation conditions because of the low coordination of the surface Ti ions of the mesoporous TiO_{2-x}.

IV. CONCLUSIONS

We have established a correlation between the metal/support interaction and catalytic activity of Pt NPs supported on a mesoporous TiO_{2-x} structure for CO oxidation probed with *in situ* investigations employing the DRIFTS technique. The Pt NPs deposited on TiO_{2-x} catalysts for CO oxidation have an enhanced catalytic activity compared with pure TiO_{2-x}, showing the important roles of the metal/support interface and oxygen vacancies in the support. Among the supported Pt catalysts, the use of TiO_{2-x} as a support material is efficient compared with nonporous oxides because its structure promotes interfacial sites and affects the metal/support interaction without any sintering effects. The linear CO band of Pt^{2+} and CO_2 adsorbed on the TiO_2 surface indicates that the activated oxygen molecule at the interface between the Pt surface and an oxygen vacancy of TiO_2 by neighboring CO molecules on the Pt surface affects the catalytic activity, which is in agreement with the DFT calculation results. Our DFT study of the origin of the experimentally observed catalytic superiority of the Pt/mesoporous TiO_{2-x} catalyst shows that the modified local electronic structure created by oxygen vacancies promotes O_2 activation and accelerates subsequent CO oxidation. The tight correlation between our experimental observations and DFT calculation results suggests the essential role of intensive modification of the chemical or physical nature of supporting oxides for the rational design of better performing catalysts. Our approach provides insight into the intrinsic origin of metal/support interactions and reaction pathways for CO oxidation on Pt-based supported catalysts and allows us to rationally design catalysts for specific applications.

SUPPLEMENTARY MATERIAL

See the supplementary material for details on DFT calculations of $Pt/TiO_2(101)$ and $Pt/TiO_{2-x}(101)$, HAADF-STEM image and EDS phase mapping of Pt/TiO_{2-x}, pore-size distribution of Pt/TiO_{2-x}, XPS analysis of the Ti 2p, Cl 2p, and Pt 4f, TEM images of Pt/TiO_{2-x} and Pt/P25 after the CO oxidation reaction, QMS results, IR of Pt/P25 under CO oxidation, DFT-calculated energetics of the sequential competitive binding of CO and O_2 on $Pt/TiO_2(101)$, and DFT calculations of CO oxidation pathways catalyzed by $Pt/TiO_2(101)$.

ACKNOWLEDGMENTS

This work was supported by the Institute for Basic Science (IBS) (Grant No. IBS-R004). H.H. and H.Y.K. appreciate the financial support from the National Research Foundation of Korea (NRF) grant funded by the Korean government (MSIP) (Grant No. NRF-2019R1A2C1089256). This research used sources from the Center for Functional Nanomaterials, which is a U.S. DOE Office of Science Facility, and the Scientific Data and Computing Center, a component of the Computational Science Initiative, at Brookhaven National Laboratory under Contract No. DE-SC0012704.

REFERENCES

[1] M. S. Chen, Y. Cai, Z. Yan, K. K. Gath, S. Axnanda, and D. W. Goodman, "Highly active surfaces for CO oxidation on Rh, Pd, and Pt," Surf. Sci. **601**, 5326–5331 (2007).
[2] G. Ertl, "Oscillatory kinetics and spatio-temporal self-organization in reactions at solid surfaces," Science **254**, 1750–1755 (1991).
[3] H. Song, R. M. Rioux, J. D. Hoefelmeyer, R. Komor, K. Niesz, M. Grass, P. Yang, and G. A. Somorjai, "Hydrothermal growth of mesoporous SBA-15 silica in the presence of PVP-stabilized Pt nanoparticles: Synthesis, characterization, and catalytic properties," J. Am. Chem. Soc. **128**, 3027–3037 (2006).
[4] M. Haruta, N. Yamada, T. Kobayashi, and S. Iijima, "Gold catalysts prepared by coprecipitation for low-temperature oxidation of hydrogen and of carbon monoxide," J. Catal. **115**, 301–309 (1989).
[5] J. Y. Park, L. R. Baker, and G. A. Somorjai, "Role of hot electrons and metal-oxide interfaces in surface chemistry and catalytic reactions," Chem. Rev. **115**, 2781–2817 (2015).
[6] G. A. Somorjai and J. Y. Park, "Molecular factors of catalytic selectivity," Angew. Chem., Int. Ed. **47**, 9212–9228 (2008).
[7] S. Tauster and S. Fung, "Strong metal-support interactions: Occurrence among the binary oxides of groups IIA–VB," J. Catal. **55**, 29–35 (1978).
[8] K. An, S. Alayoglu, N. Musselwhite, S. Plamthottam, G. Melaet, A. E. Lindeman, and G. A. Somorjai, "Enhanced CO oxidation rates at the interface of mesoporous oxides and Pt nanoparticles," J. Am. Chem. Soc. **135**, 16689–16696 (2013).

[9]S. M. Kim, K. Qadir, B. Seo, H. Y. Jeong, S. H. Joo, O. Terasaki, and J. Y. Park, "Nature of Rh oxide on Rh nanoparticles and its effect on the catalytic activity of CO oxidation," Catal. Lett. **143**, 1153–1161 (2013).
[10]Z.-Y. Pu, X.-S. Liu, A.-P. Jia, Y.-L. Xie, J.-Q. Lu, and M.-F. Luo, "Enhanced activity for CO oxidation over Pr-and Cu-doped CeO_2 catalysts: Effect of oxygen vacancies," J. Phys. Chem. C **112**, 15045–15051 (2008).
[11]I. Langmuir, "The mechanism of the catalytic action of platinum in the reactions $2Co+O_2=2Co_2$ and $2H_2+O_2=2H_2O$," Trans. Faraday Soc. **17**, 621–654 (1922).
[12]S. Polarz, J. Strunk, V. Ischenko, M. W. Van den Berg, O. Hinrichsen, M. Muhler, and M. Driess, "On the role of oxygen defects in the catalytic performance of zinc oxide," Angew. Chem., Int. Ed. **45**, 2965–2969 (2006).
[13]D. Widmann and R. Behm, "Activation of molecular oxygen and the nature of the active oxygen species for CO oxidation on oxide supported Au catalysts," Acc. Chem. Res. **47**, 740–749 (2014).
[14]I. X. Green, W. Tang, M. Neurock, and J. T. Yates, Jr., "Insights into catalytic oxidation at the Au/TiO_2 dual perimeter sites," Acc. Chem. Res. **47**, 805–815 (2013).
[15]A. Linsebigler and G. Lu, "Photocatalysis on TiO_2 surfaces: Principles, mechanisms, and selected results," Chem. Rev. **95**, 735–758 (1995).
[16]M. Menetrey, A. Markovits, and C. Minot, "Reactivity of a reduced metal oxide surface: Hydrogen, water and carbon monoxide adsorption on oxygen defective rutile $TiO_2(110)$," Surf. Sci. **524**, 49–62 (2003).
[17]N. Li, Q.-Y. Chen, L.-F. Luo, W.-X. Huang, M.-F. Luo, G.-S. Hu, and J.-Q. Lu, "Kinetic study and the effect of particle size on low temperature CO oxidation over Pt/TiO_2 catalysts," Appl. Catal., B **142**, 523–532 (2013).
[18]I. X. Green, W. Tang, M. McEntee, M. Neurock, and J. T. Yates, Jr., "Inhibition at perimeter sites of Au/TiO_2 oxidation catalyst by reactant oxygen," J. Am. Chem. Soc. **134**, 12717–12723 (2012).
[19]I. X. Green, W. Tang, M. Neurock, and J. T. Yates, "Spectroscopic observation of dual catalytic sites during oxidation of CO on a Au/TiO_2 catalyst," Science **333**, 736–739 (2011).
[20]D. Pillay and G. S. Hwang, "O_2-coverage-dependent CO oxidation on reduced $TiO_2(110)$: A first principles study," J. Chem. Phys. **125**, 144706 (2006).
[21]D. C. Sorescu, J. Lee, W. A. Al-Saidi, and K. D. Jordan, "CO_2 adsorption on $TiO_2(110)$ rutile: Insight from dispersion-corrected density functional theory calculations and scanning tunneling microscopy experiments," J. Chem. Phys. **134**, 104707 (2011).
[22]B. Yoon, H. Häkkinen, U. Landman, A. S. Wörz, J.-M. Antonietti, S. Abbet, K. Judai, and U. Heiz, "Charging effects on bonding and catalyzed oxidation of CO on Au_8 clusters on MgO," Science **307**, 403–407 (2005).
[23]G. Pacchioni, "Oxygen vacancy: The invisible agent on oxide surfaces," ChemPhysChem **4**, 1041–1047 (2003).
[24]R. Schaub, P. Thostrup, N. Lopez, E. Lægsgaard, I. Stensgaard, J. K. Nørskov, and F. Besenbacher, "Oxygen vacancies as active sites for water dissociation on rutile $TiO_2(110)$," Phys. Rev. Lett. **87**, 266104 (2001).
[25]T. L. Thompson and J. T. Yates, "TiO_2-based photocatalysis: Surface defects, oxygen and charge transfer," Top. Catal. **35**, 197–210 (2005).
[26]Z. Zhang, O. Bondarchuk, J. M. White, B. D. Kay, and Z. Dohnalek, "Imaging adsorbate O–H bond cleavage: Methanol on $TiO_2(110)$," J. Am. Chem. Soc. **128**, 4198–4199 (2006).
[27]U. Diebold, "The surface science of titanium dioxide," Surf. Sci. Rep. **48**, 53–229 (2003).
[28]S. Wendt, P. T. Sprunger, E. Lira, G. K. H. Madsen, Z. Li, J. Hansen, J. Matthiesen, A. Blekinge-Rasmussen, E. Laegsgaard, B. Hammer, and F. Besenbacher, "The role of interstitial sites in the Ti3*d* defect state in the band gap of titania," Science **320**, 1755–1759 (2008).
[29]I. Brookes, C. Muryn, and G. Thornton, "Imaging water dissociation on $TiO_2(110)$," Phys. Rev. Lett. **87**, 266103 (2001).
[30]C. Jo, Y. Seo, K. Cho, J. Kim, H. S. Shin, M. Lee, J. C. Kim, S. O. Kim, J. Y. Lee, H. Ihee, and R. Ryoo, "Random-graft polymer-directed synthesis of inorganic mesostructures with ultrathin frameworks," Angew. Chem., Int. Ed. **53**, 5117–5121 (2014).
[31]S. Xia, Z. Fu, B. Huang, J. Xu, and Z. Fan, "Ethylene/1-hexene copolymerization with $MgCl_2$-supported Ziegler–Natta catalysts containing aryloxy ligands. Part I: Catalysts prepared by immobilizing $TiCl_3$ (OAr) onto $MgCl_2$ in batch reaction," J. Mol. Catal. **355**, 161–167 (2012).
[32]S. Zhang, Y. Shao, G. Yin, and Y. Lin, "Stabilization of platinum nanoparticle electrocatalysts for oxygen reduction using poly (diallyldimethylammonium chloride)," J. Mater. Chem. **19**, 7995–8001 (2009).
[33]H. Y. Kim, M. S. Hybertsen, and P. Liu, "Controlled growth of ceria nanoarrays on anatase titania powder: A bottom-up physical picture," Nano Lett. **17**, 348–354 (2017).
[34]G. Kresse and J. Furthmuller, "Efficient iterative schemes for *ab initio* total-energy calculations using a plane-wave basis set," Phys. Rev. B **54**, 11169–11186 (1996).
[35]G. Kresse and D. Joubert, "From ultrasoft pseudopotentials to the projector augmented-wave method," Phys. Rev. B **59**, 1758–1775 (1999).
[36]J. P. Perdew and Y. Wang, "Accurate and simple analytic representation of the electron-gas correlation energy," Phys. Rev. B **45**, 13244–13249 (1992).
[37]S. L. Dudarev, G. A. Botton, S. Y. Savrasov, C. J. Humphreys, and A. P. Sutton, "Electron-energy-loss spectra and the structural stability of nickel oxide: An LSDA+U study," Phys. Rev. B **57**, 1505–1509 (1998).
[38]J. B. Park, J. Graciani, J. Evans, D. Stacchiola, S. G. Ma, P. Liu, A. Nambu, J. F. Sanz, J. Hrbek, and J. A. Rodriguez, "High catalytic activity of $Au/CeOx/TiO_2(110)$ controlled by the nature of the mixed-metal oxide at the nanometer level," Proc. Natl. Acad. Sci. U. S. A. **106**, 4975–4980 (2009).
[39]G. Henkelman and H. Jónsson, "Improved tangent estimate in the nudged elastic band method for finding minimum energy paths and saddle points," J. Chem. Phys. **113**, 9978–9985 (2000).
[40]G. Henkelman, B. P. Uberuaga, and H. Jónsson, "A climbing image nudged elastic band method for finding saddle points and minimum energy paths," J. Chem. Phys. **113**, 9901–9904 (2000).
[41]S. H. Kim, C.-H. Jung, N. Sahu, D. Park, J. Y. Yun, H. Ha, and J. Y. Park, "Catalytic activity of Au/TiO_2 and Pt/TiO_2 nanocatalysts prepared with arc plasma deposition under CO oxidation," Appl. Catal., A **454**, 53–58 (2013).
[42]S. Watanabe, X. Ma, and C. Song, "Characterization of structural and surface properties of nanocrystalline TiO_2–CeO_2 mixed oxides by XRD, XPS, TPR, and TPD," J. Phys. Chem. C **113**, 14249–14257 (2009).
[43]Y. Zhou, D. E. Doronkin, M. Chen, S. Wei, and J.-D. Grunwaldt, "Interplay of Pt and crystal facets of TiO_2: CO oxidation activity and *operando* XAS/DRIFTS studies," ACS Catal. **6**, 7799–7809 (2016).
[44]G. Liu, H. G. Yang, X. Wang, L. Cheng, H. Lu, L. Wang, G. Q. Lu, and H.-M. Cheng, "Enhanced photoactivity of oxygen-deficient anatase TiO_2 sheets with dominant {001} facets," J. Phys. Chem. C **113**, 21784–21788 (2009).
[45]M. W. Shah, Y. Zhu, X. Fan, J. Zhao, Y. Li, S. Asim, and C. Wang, "Facile synthesis of defective TiO_{2-x} nanocrystals with high surface area and tailoring bandgap for visible-light photocatalysis," Sci. Rep. **5**, 15804 (2015).
[46]I. Luciu, R. Bartali, and N. Laidani, "Influence of hydrogen addition to an Ar plasma on the structural properties of TiO_{2-x} thin films deposited by RF sputtering," J. Phys. D: Appl. Phys. **45**, 345302 (2012).
[47]X. Xue, R. Chen, H. Chem, Y. Hu, Q. Ding, Z. Liu, L. Ma, G. Zhu, W. Zhang, Q. Yu, J. Liu, J. Ma, and Z. Jin, "Oxygen vacancy engineering promoted photocatalyic ammonia synthesis on ultrathin two-dimensional bismuth oxybromide nanosheets," Nano Lett. **18**, 7372–7377 (2018).
[48]G. Zhang, Z. Hu, M. Sun, Y. Liu, L. Liu, H. Liu, C. Huang, J. Qu, and J. Li, "Formation of Bi_2WO_6 bipyramids with vacancy pairs for enhanced solar-driven photoactivity," Adv. Funct. Mater. **25**, 3726 (2015).
[49]J. Su, C. Xie, C. Chen, Y. Yu, G. Kennedy, G. A. Somorjai, and P. Yang, "Insights into the mechanism of tandem alkene hydroformylation over a nanostructured catalyst with multiple interfaces," J. Am. Chem. Soc. **138**, 11568–11574 (2016).
[50]K. An, S. Alayoglu, N. Musselwhite, K. Na, and G. A. Somorjai, "Designed catalysts from Pt nanoparticles supported on macroporous oxides for selective isomerization of *n*-hexane," J. Am. Chem. Soc. **136**, 6830–6833 (2014).
[51]X. Liu, J. Iocozzia, Y. Wang, X. Cui, Y. Chen, S. Zhao, Z. Li, and Z. Lin, "Noble metal-metal oxide nanohybrids with tailored nanostructures for efficient solar energy conversion, photocatalysis and environmental remediation," Energy Environ. Sci. **10**, 402–434 (2017).

[52]S. Mandal, D. Roy, R. V. Chaudhari, and M. Sastry, "Pt and Pd nanoparticles immobilized on amine-functionalized zeolite: Excellent catalysts for hydrogenation and Heck reactions," Chem. Mater. **16**, 3714–3724 (2004).
[53]S. Oh, Y. K. Kim, C. H. Jung, W. H. Doh, and J. Y. Park, "Effect of the metal–support interaction on the activity and selectivity of methanol oxidation over Au supported on mesoporous oxides," Chem. Commun. **54**, 8174–8177 (2018).
[54]L. Di, D. Duan, X. Zhang, B. Qi, and Z. Zhang, "Effect of TiO_2 crystal phase and preparation method on the catalytic performance of Au/TiO_2 for CO oxidation," IEEE Trans. Plasma Sci. **44**, 2692 (2016).
[55]M. A. Albiter and F. Zaera, "Adsorption properties of supported platinum catalysts prepared using dendrimers," Langmuir **26**, 16204–16210 (2010).
[56]K. Ding, A. Gulec, A. M. Johnson, N. M. Schweitzer, G. D. Stucky, L. D. Marks, and P. C. Stair, "Identification of active sites in CO oxidation and water-gas shift over supported Pt catalysts," Science **350**, 189–192 (2015).
[57]J. Sirita, S. Phanichphant, and F. C. Meunier, "Quantitative analysis of adsorbate concentrations by diffuse reflectance FT-IR," Ann. Chem. **79**, 3912–3918 (2007).
[58]A. D. Allian, K. Takanabe, K. L. Fujdala, X. Hao, T. J. Truex, J. Cai, C. Buda, M. Neurock, and E. Iglesia, "Chemisorption of CO and mechanism of CO oxidation on supported platinum nanoclusters," J. Am. Chem. Soc. **133**, 4498–4517 (2011).
[59]J. Xu and J. T. Yates, Jr., "Terrace width effect on adsorbate vibrations: A comparison of Pt(335) and Pt(112) for chemisorption of CO," Surf. Sci. **327**, 193–201 (1995).
[60]R. Shigeishi and D. A. King, "Chemisorption of carbon monoxide on platinum {111}: Reflection-absorption infrared spectroscopy," Surf. Sci. **58**, 379–396 (1976).
[61]F. Boccuzzi, A. Chiorino, M. Manzoli, P. Lu, T. Akita, S. Ichikawa, and M. Haruta, "Au/TiO_2 nanosized samples: A catalytic, TEM, and FTIR study of the effect of calcination temperature on the CO oxidation," J. Catal. **202**, 256–267 (2001).
[62]P. Carlsson, L. Osterlund, P. Thormahlen, A. Palmqvist, E. Fridell, J. Jansson, and M. Skoglundh, "A transient *in situ* FTIR and XANES study of CO oxidation over Pt/AlO catalysts," J. Catal. **226**, 422–434 (2004).
[63]J. Ke, W. Zhu, Y. Jiang, R. Si, Y.-J. Wang, S.-C. Li, C. Jin, H. Liu, W.-G. Song, C.-H. Yan, and Y.-W. Zhang, "Strong local coordination structure effects on subnanometer PtO_x clusters over CeO_2 nanowires probed by low-temperature CO oxidation," ACS Catal. **5**, 5164–5173 (2015).
[64]C. Lentz, S. P. Jand, J. Melke, C. Roth, and P. Kaghazchi, "DRIFTS study of CO adsorption on Pt nanoparticles supported by DFT calculations," J. Mol. Catal. A: Chem. **426**, 1–9 (2017).
[65]A. Martinez-Arias, J. Coronado, R. Cataluna, J. Conesa, and J. Soria, "Influence of mutual platinum-dispersed ceria interactions on the promoting effect of ceria for the CO oxidation reaction in a Pt/CeO_2/Al_2O_3 catalyst," J. Phys. Chem. B **102**, 4357–4365 (1998).
[66]M. J. Kale and P. Christopher, "Utilizing quantitative *in situ* FTIR spectroscopy to identify well-coordinated Pt atoms as the active site for CO oxidation on Al_2O_3-supported Pt catalysts," ACS Catal. **6**, 5599–5609 (2016).
[67]X. Lin, B. Yang, H.-M. Benia, P. Myrach, M. Yulikov, A. Aumer, M. A. Brown, M. Sterrer, O. Bondarchuk, and E. Kieseritzky, "Charge-mediated adsorption behavior of CO on MgO-supported Au clusters," J. Am. Chem. Soc. **132**, 7745–7749 (2010).
[68]J. Lee, Y. Ryou, X. Chan, T. J. Kim, and D. H. Kim, "How Pt interacts with CeO_2 under the reducing and oxidizing environments at elevated temperature: The origin of improved thermal stability of Pt/CeO_2 compared to CeO_2," J. Phys. Chem. C **120**, 25870–25879 (2016).
[69]J. A. Farmer and C. T. Campbell, "Ceria maintains smaller metal catalyst particles by strong metal-support bonding," Science **329**, 933–936 (2010).
[70]A. Linsebigler, G. Lu, and J. T. Yates, "CO photooxidation on TiO_2(110)," J. Phys. Chem. **100**, 6631–6636 (1996).
[71]G. Lu, A. Linsebigler, and J. T. Yates, Jr., "The adsorption and photodesorption of oxygen on the TiO_2(110) surface," J. Chem. Phys. **102**, 4657–4662 (1995).
[72]F. Boccuzzi and A. Chiorino, "FTIR study of CO oxidation on Au/TiO_2 at 90 K and room temperature. An insight into the nature of the reaction centers," J. Phys. Chem. B **104**, 5414–5416 (2000).
[73]J. D. Henao, T. Caputo, J. H. Yang, M. C. Kung, and H. H. Kung, "*In situ* transient FTIR and XANES studies of the evolution of surface species in CO oxidation on Au/TiO_2," J. Phys. Chem. B **110**, 8689–8700 (2006).
[74]L.-F. Liao, C.-F. Lien, D.-L. Shieh, M.-T. Chen, and J.-L. Lin, "FTIR study of adsorption and photoassisted oxygen isotopic exchange of carbon monoxide, carbon dioxide, carbonate, and formate on TiO_2," J. Phys. Chem. B **106**, 11240–11245 (2002).
[75]L. DeRita, S. Dai, K. Lopez-Zepeda, N. Pham, G. W. Graham, X. Pan, and P. Christopher, "Catalyst architecture for stable single atom dispersion enables site-specific spectroscopic and reactivity measurements of CO adsorbed to Pt atoms, oxidized Pt clusters, and metallic Pt clusters on TiO_2," J. Am. Chem. Soc. **139**, 14150–14165 (2017).
[76]Q. Fu, W.-X. Li, Y. Yao, H. Liu, H.-Y. Su, D. Ma, X.-K. Gu, L. Chen, Z. Wang, and H. Zhang, "Interface-confined ferrous centers for catalytic oxidation," Science **328**, 1141–1144 (2010).
[77]S. Oh, S. Back, W. H. Doh, S. Y. Moon, J. Kim, Y. Jung, and J. Y. Park, "Probing surface oxide formations on SiO_2-supported platinum nanocatalysts under CO oxidation," RSC Adv. **7**, 45003–45009 (2017).
[78]Z. Duan and G. Henkelman, "Calculations of CO oxidation over a Au/TiO_2 catalyst: A study of active sites, catalyst deactivation, and moisture effects," ACS Catal. **8**, 1376–1383 (2018).
[79]M. Kotobuki, R. Leppelt, D. Hansgen, D. Widmann, and R. Behm, "Reactive oxygen on a Au/TiO_2 supported catalyst," J. Catal. **264**, 67–76 (2009).
[80]H. Ha, S. Yoon, K. An, and H. Y. Kim, "Catalytic CO oxidation over Au nanoparticles supported on CeO_2 nanocrystals: Effect of the Au–CeO_2 interface," ACS Catal. **8**, 11491–11501 (2018).
[81]H. Y. Kim and G. Henkelman, "CO oxidation at the interface of Au nanoclusters and the stepped-CeO_2 (111) surface by the Mars-van Krevelen mechanism," J. Phys. Chem. Lett. **4**, 216–221 (2013).
[82]G. N. Vayssilov, Y. Lykhach, A. Migani, T. Staudt, G. P. Petrova, N. Tsud, T. Skala, A. Bruix, F. Illas, K. C. Prince, V. Matolin, K. M. Neyman, and J. Libuda, "Support nanostructure boosts oxygen transfer to catalytically active platinum nanoparticles," Nat. Mater. **10**, 310–315 (2011).
[83]D. Widmann and R. J. Behm, "Active oxygen on a Au/TiO_2 catalyst: Formation, stability, and CO oxidation activity," Angew. Chem., Int. Ed. **50**, 10241–10245 (2011).
[84]H. Ha, H. An, M. Yoo, J. Lee, and H. Y. Kim, "Catalytic CO oxidation by CO-saturated Au nanoparticles supported on CeO_2: Effect of CO coverage," J. Phys. Chem. C **121**, 26895–26902 (2017).
[85]K. Shin, L. Zhang, H. An, H. Ha, M. Yoo, H. M. Lee, G. Henkelman, and H. Y. Kim, "Interface engineering for a rational design of poison-free bimetallic CO oxidation catalysts," Nanoscale **9**, 5244–5253 (2017).